Journal of
Applied
Crystallography

ISSN 1600-5767

Received 22 July 2014
Accepted 11 February 2015

Determination of the melting and freezing temperatures of Pb nanoparticles embedded in a $PbO–B_2O_3–SnO_2$ glass by using only the SAXS method

G. Kellermann,[a]* A. Gorgeski,[a] A. F. Craievich[b] and L. A. Montoro[c]

[a]Departamento de Física, Universidade Federal do Paraná, Curitiba, PR, Brazil, [b]Instituto de Física, Universidade de São Paulo, SP, Brazil, and [c]Departamento de Química, Universidade Federal de Minas Gerais, Belo Horizonte, MG, Brazil. Correspondence e-mail: keller@fisica.ufpr.br

Melting and freezing of metallic nanoparticles embedded in glass matrices usually occur at temperatures lower than for the same metal in the bulk state. *In situ* small-angle X-ray scattering (SAXS) measurements using a synchrotron beamline and a specially designed high-temperature chamber allowed the determination of the temperature dependence of the SAXS intensity produced by a dilute and nearly monodisperse set of spherical Pb nanoparticles, with an average radius $\langle R\rangle$ = 16.1 nm, embedded in a homogeneous lead–borate oxide glass. The temperature dependences of the nanoparticle volume $V(T)$ and nanoparticle radius of gyration $R_g(T)$ derived from SAXS results exhibit clear discontinuities during the cooling and during the heating processes, thus allowing for precise determinations of the melting and freezing temperatures of the studied Pb nanoparticles. Additional features observed in both $V(T)$ and $R_g(T)$ curves showed that during the heating cycle the frozen Pb nanoparticles suffer a transition to a more compact phase at 433 K before melting at 580 K. The results of this work demonstrate that the melting and freezing temperatures of nanoparticles in a very diluted state – for which the X-ray diffraction technique is not sensitive enough – can be precisely determined by applying only the SAXS method.

1. Introduction

The formation of metallic and semiconductor nanoparticles embedded in glass matrices has attracted the attention of many scientists (Gonella & Mazzoldi, 2000; Craievich *et al.*, 2002; Nogami & Abe, 1994; Yang *et al.*, 2005; Hamanaka & Nakamura, 1999). The reasons for this are related to interesting basic aspects of the properties of nanostructured materials, which often exhibit unusual features, and also to the fact that they are potential candidates for the development of new optoelectronic devices (Mazzoldi *et al.*, 1996; Pavesi *et al.*, 2000).

The first step for an adequate understanding of the physical properties of nanomaterials composed of a homogeneous matrix in which isolated nanoparticles are embedded is to properly characterize the relevant structural features of the nanoparticles, namely the shape, atomic structure and size distribution.

Several techniques are commonly used to experimentally determine the liquid-to-solid (freezing) and solid-to-liquid (melting) transitions of nanoparticles embedded in homogeneous matrices or supported on substrates (Takagi, 1954; Kofman *et al.*, 1990; Zhao *et al.*, 2001, and references therein; Kellermann & Craievich, 2002, 2008; Itoigawa *et al.*, 1997; Lopeandia & Rodriguez-Viejo, 2007; Valov & Leiman, 1997; Cheyssac *et al.*, 1988). Some of these techniques, such as X-ray diffraction (XRD) (Kellermann & Craievich, 2002) and electron diffraction (Takagi, 1954), are sensitive to the atomic arrangement inside the nanoparticles, thus allowing one to distinguish between crystalline and liquid or amorphous (disordered) structures. Others often applied are based on a combination of transmission electron microscopy (TEM) and thermal (Itoigawa *et al.*, 1997; Lopeandia & Rodriguez-Viejo, 2007) or optical (Valov & Leiman, 1997; Cheyssac *et al.*, 1988) analysis of the studied materials during heating and cooling processes.

In a previous investigation the melting and freezing of Bi nanocrystals embedded in glass were investigated by simultaneous use of small-angle X-ray scattering (SAXS) and XRD (Kellermann & Craievich, 2008). The correlation observed in the behaviors of XRD and SAXS patterns showed that the measurement of SAXS intensity curves as a function of temperature is a useful method to investigate the phase transitions of nanoparticles embedded in glass matrices. It was established in this study that discontinuities in the integrated SAXS intensity *versus* temperature curves at the crystal-to-liquid and liquid-to-crystal transitions – a consequence of the

change in volume and density of the nanoparticles – lead to a precise determination of the melting and freezing temperatures of the nanoparticles.

In this work we have performed high-resolution transmission electron microscopy (HRTEM), XRD and SAXS analyses of the structure of a diluted set of Pb nanoparticles embedded in a $PbO–B_2O_3–SnO_2$ glass. As will be explained later, while TEM images taken at room temperature allowed us to clearly establish the presence of spherical Pb nanoparticles embedded in the glass, the corresponding XRD patterns of the same samples did not exhibit any Bragg peak expected for crystalline Pb nanoparticles. This demonstrated that the sensitivity of the XRD technique is not in this case high enough to allow an adequate analysis of the diluted set of Pb nanoparticles studied here. On the other hand, the results from SAXS measurements yielded the temperature dependence of low-resolution parameters related to the size of the nanoparticles, which allowed us to characterize relevant aspects of melting and freezing transitions.

The use of SAXS instead of wide-angle X-ray diffraction procedures for the characterization of phase transitions of metallic particles is not frequently described in the literature. An investigation that applied the small-angle neutron scattering (SANS) technique to the characterization of phase transitions of Pb particles in an Al crystalline matrix has recently been published (Strunz *et al.*, 2012). Notice that the SAXS and SANS techniques are sensitive to the size of particles in the nanometre size range irrespective of their internal atomic arrangements, namely crystalline or amorphous. Therefore, provided the particles exhibit a not vanishing volume variation at the transitions, the SAXS or SANS techniques can be applied to characterize freezing and melting transformations even in cases in which the solid particles are in disordered (not crystalline) states.

2. Sample preparation and SAXS/XRD setup

A $52PbO–45B_2O_3–3SnO_2$ glass was prepared by initially melting together the glass-forming reagents PbO, B_2O_3 and SnO at 1053 K under vacuum for 1 h. SnO was added in order to reduce a small fraction of the PbO species, thus leading to the formation of SnO_2 and isolated metallic Pb atoms, both homogeneously dispersed in the $PbO–B_2O_3$ mixture.

The melt was then fast-quenched down to room temperature using a splat-cooling device (Kellermann & Craievich, 2002, 2008). This procedure allowed us to obtain at room temperature a homogeneous glass platelet with a thickness t = 70 μm.

After quenching, the Pb-doped $52PbO–45B_2O_3–3SnO_2$ glass was subjected to isothermal annealing for 35 min at high temperature, T_{iso} = 716 K. The initially isolated Pb atoms, being non-miscible in the glass oxide matrix, segregate and by 'up-hill' atomic diffusion promote the homogeneous nucleation and growth of a diluted set of Pb nanoparticles embedded in the homogeneous glass. Since the annealing temperature is much higher than the melting temperature of bulk Pb, T_m = 600 K, the isothermal annealing at 716 K led to the formation and growth of spherical liquid Pb nanodroplets embedded in the glass.

In order to characterize the temperature effect on the low-resolution structure of the Pb nanoparticles and determine their melting and freezing transition temperatures, *in situ* SAXS measurements were performed. The glass sample containing Pb nanoparticles was placed inside a specially designed high-temperature cell (Kellermann *et al.*, 2003) and subjected to a cooling/heating cycle. The maximum temperature that the sample reaches during the cooling/heating cycle is T_{max} = 650 K, well below the temperature of the previous isothermal process of nanoparticle growth (T_{iso} = 716 K); thus no significant additional growth of Pb nanoparticles is expected to occur during the whole cooling/heating cycle.

SAXS measurements were performed using the SAXS2 beamline of the synchrotron laboratory LNLS, Campinas, Brazil. A monochromatic and focused X-ray beam with a point-like cross section and wavelength equal to λ = 0.10781 nm and a 2D MAR-165 CCD photon detector were employed. Because of the small X-ray beam cross section of the incoming beam no mathematical desmearing of the experimental curves was needed. The high-temperature cell used for *in situ* SAXS experiments (Kellermann *et al.*, 2003) consists of a main volume under vacuum, a pre-chamber and an electronic device for temperature control. The chamber has two windows for entrance and exit of the incident and scattered SAXS beams, respectively, and a third Kapton window for simultaneous recording of X-ray diffraction patterns over the $15 < 2\theta < 160^\circ$ range.

3. SAXS intensity from nanoparticles embedded in a homogeneous matrix. Basic theory

For a simple isotropic 'two electron-density model', consisting of a diluted and polydisperse set of spherical particles having electron density ρ_{np} embedded in an also homogeneous matrix with electron density ρ_m, the SAXS intensity is given by (Craievich, 2005)

$$I(q) = (\rho_{np} - \rho_m)^2 \left(\frac{4\pi}{3}\right)^2 \int |F(q)|^2 N(R) R^6 \, dR, \qquad (1)$$

where the frequency of the nanoparticle radius is represented by the radius distribution function $N(R)$. The function $|F(q)|^2$ is the normalized form factor of a homogeneous spherical particle having a radius R, given by (Craievich, 2005)

$$|F(q)|^2 = \left[3\frac{\sin(qR) - qR\sin(qR)}{(qR)^3}\right]^2. \qquad (2)$$

The integral of SAXS intensity $I(q)$ in reciprocal space, Q, is related to the total volume occupied by nanoparticles in the glass V_{np} by (Craievich, 2005)

$$Q = \int 4\pi q^2 I(q) \, dq = (2\pi)^3 (\rho_{np} - \rho_m)^2 V_{np} \qquad (3)$$

or

$$Q \propto (\rho_{np} - \rho_m)^2/\rho_{np}. \quad (4)$$

Across structural phase transitions the SAXS intensity exhibits a sharp variation due to the expected change in mass density and volume of the nanoparticles at the transitions, while the matrix mass density remains essentially constant. The differentiation of equation (4) allows one to obtain an expression for the relative variation in the mass density $\delta\rho_{np}/\rho_{np}$ and volume $\delta V_{np}/V_{np}$ of the nanoparticles, at the transition temperatures, as functions of the relative variation of the integrated SAXS intensity $\delta Q/Q$:

$$\frac{\delta\rho_{np}}{\rho_{np}} = -\frac{\delta V_{np}}{V_{np}} = \left(\frac{\rho_{np} - \rho_m}{\rho_{np} + \rho_m}\right)\frac{\delta Q}{Q}. \quad (5)$$

Notice that for $\rho_{np} > \rho_m$ the factor between parentheses is positive, thus indicating in this case opposite trends for $\delta V_{np}/V_{np}$ and $\delta Q/Q$ at the transitions. For the particular case of free nanoparticles, *i.e.* for $\rho_m = 0$, equation (5) simply becomes $\delta V_{np}/V_{np} = -\delta Q/Q$.

The ρ_{np} and ρ_m electron densities can be calculated from $\rho_{np} = (Z_{Pb}/M_{Pb})\rho_{Pb}^m$ and $\rho_m = (Z/M)_g\rho_g^m$, where Z_{Pb} and M_{Pb} are the atomic number and atomic mass of Pb, $(Z/M)_g$ is the average value of the ratio between the atomic number and the atomic mass of atoms in the glass, and ρ_{Pb}^m and ρ_g^m are the specific masses of nanoparticles and glass, respectively.

Another function that can be determined from SAXS measurements is the temperature dependence of the radius of gyration of the nanoparticles, $R_g(T)$. This parameter is derived from the low-q limit of the experimental SAXS curve associated with a dilute set of identical nanoparticles, by applying Guinier's law:

$$I(q) = I(0)\exp\left(-\frac{1}{3}R_g^2q^2\right). \quad (6)$$

The radius of gyration is experimentally derived as $R_g = (3|\alpha|)^{1/2}$, where α is the slope in the linear part of Guinier plots, ln $I(q)$ *versus* q^2. For spherical nanoparticles their radius R is equal to $(5/3)^{1/2}R_g$. Notice that for nanoparticles with size dispersion the radius of gyration derived by applying Guinier's law is an average that weights large nanoparticles more (Craievich, 2005).

4. Experimental results

4.1. HRTEM characterization of Pb nanoparticles at room temperature

As mentioned before, the initially homogeneous splat-quenched $52PbO–45B_2O_3–3SnO_2$ glass doped with Pb atoms was held for 35 min at 716 K. Since Pb atoms are not miscible in the glass matrix at this temperature, which is well above the melting temperature of bulk Pb (T_m = 600.1 K), the isothermal annealing at 716 K is expected to promote the formation of liquid Pb nanodroplets embedded in the glass matrix.

After being cooled to room temperature (T = 300 K), the glass sample containing frozen Pb nanoparticles was studied by high-resolution TEM. Fig. 1(*a*) shows an HRTEM image of a representative fraction of the studied glass taken at room temperature. The image in Fig. 1(*a*) clearly indicates the presence of well defined and nearly spherical crystalline nanoparticles, exhibiting a clear contrast with respect to the surrounding amorphous glass matrix. The phase-contrast HRTEM images reveal the presence of crystalline nano-

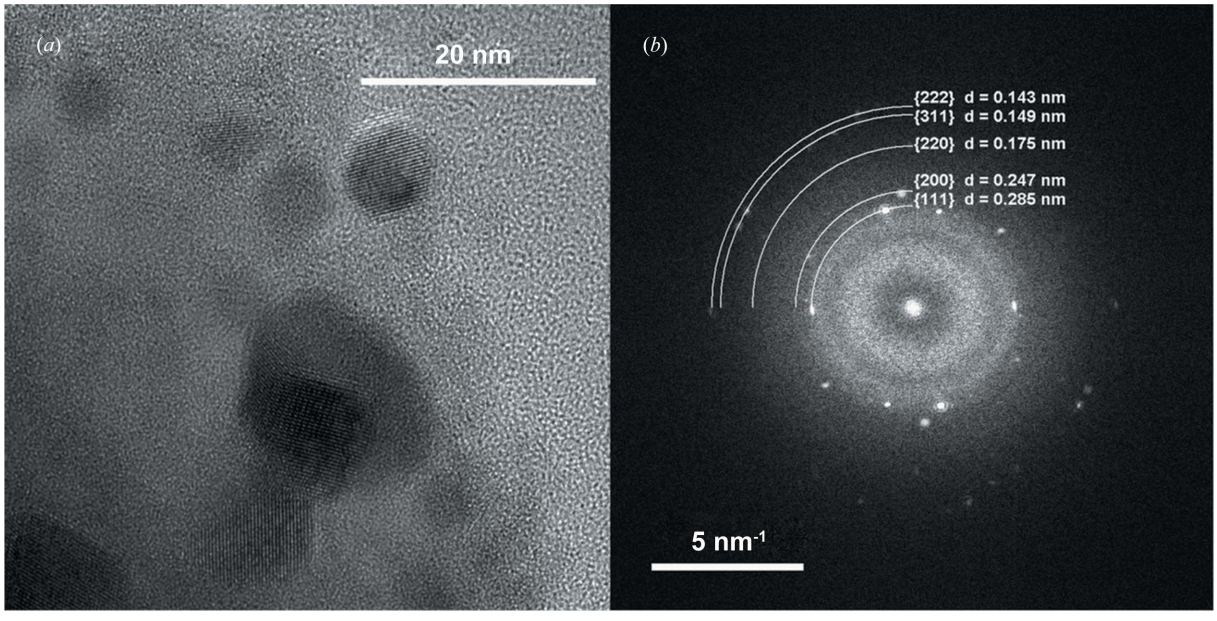

Figure 1
(*a*) High-resolution TEM image showing nearly spherical Pb nanocrystals embedded in the lead–borate glass and (*b*) fast Fourier transform of the same image showing the expected positions of the electron diffraction spots. The circles in (*b*) indicate the expected electron powder diffraction rings corresponding to Pb crystals with an f.c.c. crystallographic lattice.

particles evidenced by atomic fringes or planes on properly oriented particles.

In order to study the crystallographic structure of Pb nanoparticles a fast Fourier transform (FFT) of the HRTEM image (Fig. 1*a*) was applied and then the lattice spacing was determined. Fig. 1(*b*) shows the indexed FFT pattern, where the spots in this image correspond to the positions expected for the electron diffraction Bragg peaks associated with an *Fm*3*m* face-centered cubic (f.c.c.) Pb lattice. This result clearly indicates that the studied sample contains Pb nanocrystals with a regular *Fm*3*m* structure embedded in the amorphous glass matrix.

4.2. XRD analysis at room temperature

In order to achieve a more detailed characterization of the Pb nanoparticles, XRD measurements were performed at room temperature (T = 300 K) and also at 650 K, this last temperature being well above the melting temperature of bulk Pb (600.1 K). The recorded XRD diffractogram measured at room temperature is displayed in Fig. 2, together with vertical lines corresponding to the XRD pattern expected for crystalline bulk Pb. The X-ray diffraction pattern plotted in Fig. 2 exhibits the broad halo produced by the glass matrix and a few superposed weak Bragg peaks. The Bragg angles of the diffraction peaks do not match those expected for bulk Pb crystals or those derived from the result of our analysis of an HRTEM image (Fig. 1*b*). These same peaks with nearly the same intensities were also observed in the as-quenched glass, *i.e.* before the thermal treatment used to promote the formation and growth of Pb nanoparticles (716 K), and at 650 K. These results thus safely confirm that the observed Bragg peaks are not related to X-ray scattering produced by Pb nanocrystals. We have assigned the weak Bragg peaks shown in Fig. 2 to the presence of a minor volume fraction of a crystalline phase developed in the glass matrix during the cooling process.

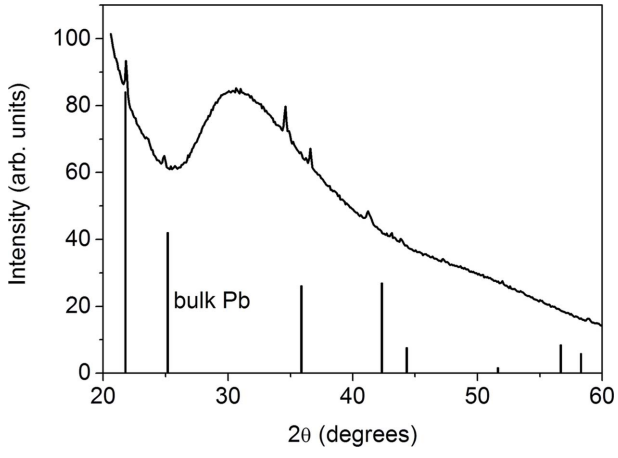

Figure 2
XRD pattern of the studied lead–borate glass containing solid Pb nanoparticles recorded at room temperature. The angular position and relative intensity of the Bragg peaks corresponding to cubic bulk Pb (ICDD/JCPDF 4-686) are indicated by vertical lines.

The absence of Bragg peaks associated with crystalline Pb in the XRD pattern at room temperature may be related to the fact that a very low fraction of the total volume is occupied by the nanocrystals or, alternatively, to an eventual formation after freezing of a metastable disordered solid structure instead of a well ordered crystalline structure as *a priori* expected. Since the Bragg peaks corresponding to crystalline Pb were not detected in our XRD patterns, we have discarded the use of this technique for the structural characterization of the freezing and melting temperatures of the studied Pb nanoparticles.

4.3. Determination of the radius distribution of spherical Pb droplets by SAXS

The initial homogeneous glass sample was held for 35 min at 716 K to promote the formation of Pb nanoparticles and then studied by SAXS before cooling to room temperature. As mentioned before, since the melting temperature of bulk Pb is 600.1 K, we expect the Pb nanoparticles studied by SAXS at 716 K to be in the liquid state. Fig. 3 displays the SAXS intensity produced by the Pb nanodroplets. The oscillations that can be observed in the scattering intensity correspond to those predicted by the form factor for spherical nanoparticles [equation (2)] and qualitatively suggest that the liquid nanodroplets exhibit a rather narrow radius distribution.

In order to determine the radius distribution function $N(R)$ of the Pb nanodroplets held at 716 K, the experimental SAXS intensity in Fig. 3 was modeled using equations (1) and (2). The best agreement with the experimental SAXS curve was obtained using a Gaussian function for the radius distribution $N(R)$. From the best fitting procedure the average radius that resulted was $\langle R \rangle$ = 16.1 nm and the standard deviation of the radius distribution function was σ = 0.16 nm. The experimental and modeled SAXS curves and the $N(R)$ function determined by the best fitting procedure are displayed in Fig. 3.

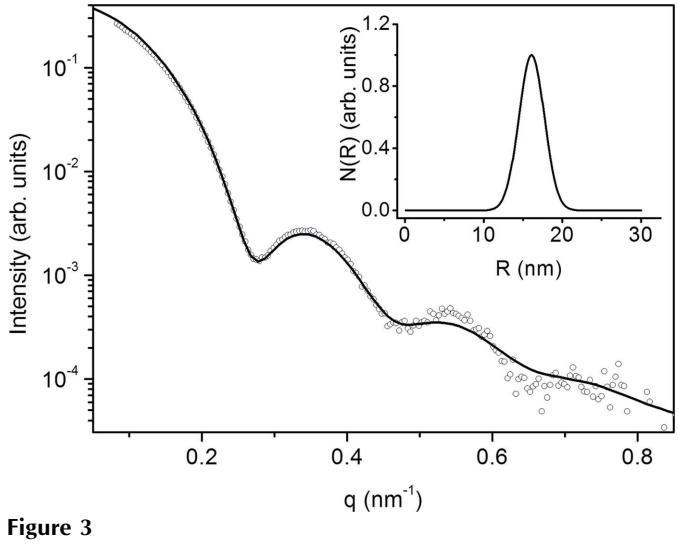

Figure 3
Experimental SAXS intensity produced by Pb nanodroplets embedded in a lead–borate glass (open circles) and modeled SAXS curve determined from a best fitting procedure using equations (1) and (2) (continuous line). Inset: radius distribution function of spherical Pb nanodroplets determined by applying the best fitting procedure described in the text.

4.4. SAXS intensity at varying temperatures. Determination of melting and freezing temperatures of Pb nanoparticles

Since our XRD analysis was not sensitive enough for determination of the melting and freezing temperatures of the studied dilute set of Pb nanoparticles in glass, we have tried to derive this information by applying the SAXS method. In spite of the fact that SAXS only provides low-resolution structural parameters, not being sensitive to the detailed atomic arrangement inside the nanoparticles, this technique was expected to be useful for detecting small but sharp variations in nanoparticle volume at the phase transitions. In addition, the SAXS technique is particularly useful for the study of very dilute systems because it probes all nanoparticles, while in XRD only a small fraction of them produce Bragg *hkl* peaks, *i.e.* those with their *hkl* planes properly oriented with respect to the incident beam.

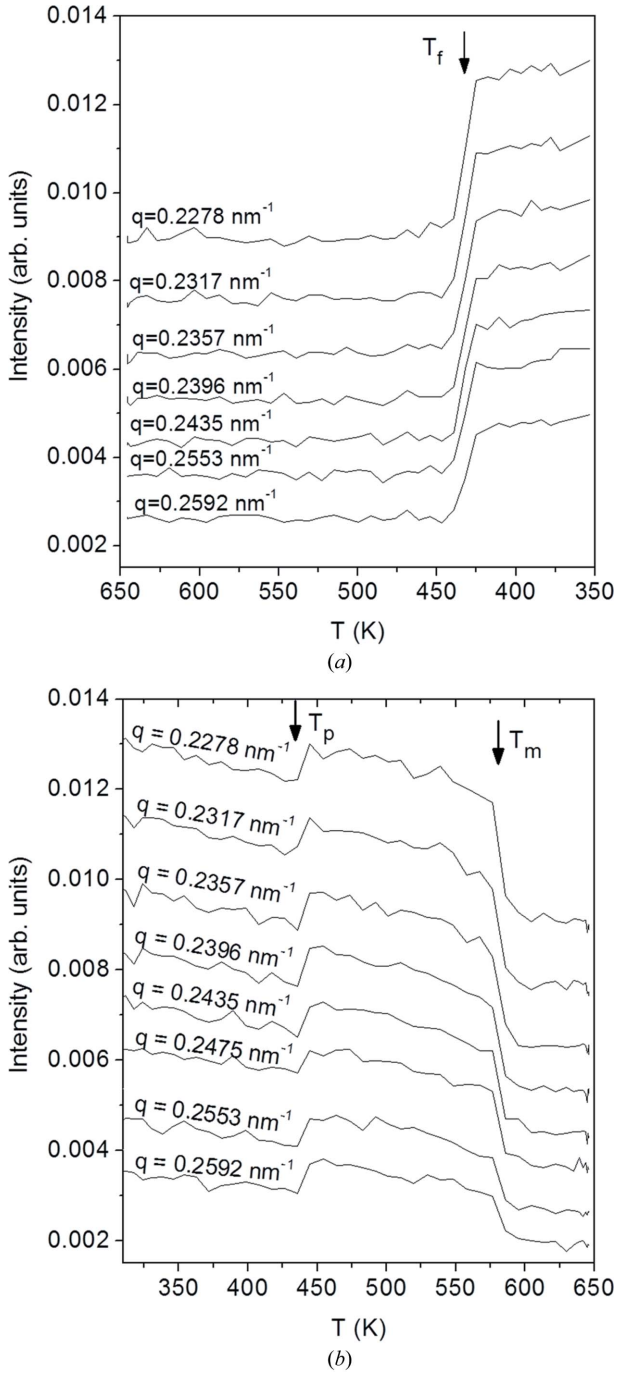

Figure 4
SAXS intensity as a function of temperature for the indicated q values during the cooling (a) and the heating (b) stages of the thermal cycle. The arrows T_f and T_m point to the discontinuities in SAXS intensity associated with the freezing and melting, respectively, of Pb nanoparticles. T_p indicates the temperature of a pre-transition that occurs during the heating stage of the thermal cycle.

Fig. 4(a) exhibits the temperature dependence of the SAXS intensity at different q values during the cooling process. We can notice that on cooling the SAXS intensities, for every q, exhibit a sharp increase for decreasing temperatures at T = 433 K. This sharp increase of SAXS intensity observed at T = 433 K under cooling was assigned to the decrease in nanoparticle sizes associated with the freezing of liquid Pb droplets.

The intensity curves for a given q value during the heating process are plotted in Fig. 4(b). The main discontinuity in the $I(q_i,T)$ curves, which occurs at T = 580 K, was assigned to the increase in volume of the Pb nanoparticles expected at their melting temperature.

In short, these simple SAXS measurements at varying temperatures yielded precise determinations of the melting temperature, T_m = 580 K, and freezing temperature, T_f = 433 K, of Pb nanoparticles with an average radius $\langle R\rangle$ = 16.1 nm embedded in a $PbO–B_2O_3–SnO_2$ glass.

Another sharp discontinuity in SAXS intensity is apparent in Fig. 4(b) at T = 433 K, *i.e.* at the same temperature as that of freezing of Pb droplets during cooling (Fig. 4a). This *a priori* unexpected effect related to the increase in SAXS intensity at T = 433 K will be discussed later.

4.5. Temperature dependences of the integral of SAXS intensity and size of Pb nanoparticles

For increasing temperatures, the electron densities of Pb nanoparticles, ρ_{np}, and the matrix, ρ_m, are expected to exhibit a continuous and decreasing trend due to thermal expansion. In addition a sharp decrease in the density of nanoparticles, ρ_{np}, is expected at their melting temperature. For the volume of the nanoparticles, V_{np}, which is inversely proportional to the density, an opposite trend is expected. Furthermore, we have tried to extract additional information about the structural phase transitions of Pb nanoparticles by analyzing details of the whole SAXS curves measured during a cooling/heating cycle.

We calculated the temperature dependence of the integrated SAXS intensity, $Q(T)$, by applying equation (3) to the experimental SAXS curves measured at different temperatures. On the other hand, the radii of gyration of the Pb nanoparticles were determined by applying the Guinier law, equation (6), to the low-q range of SAXS intensity curves. Both functions, $Q(T)$ and $R_g(T)$, were determined for samples submitted to cooling and heating processes, and they are plotted in Figs. 5(a) and 5(b), respectively.

For the cooling stage of the thermal cycle, we can clearly notice in Figs. 5(a) and 5(b), at T = 433 K, a sharp increase in $Q(T)$ and also a sharp decrease in $R_g(T)$ for decreasing

Table 1
Transition temperatures and relative variations in volume and average Guinier radius corresponding to the melting and freezing of Pb nanoparticles with an average radius $\langle R \rangle$ = 16.1 nm.

The transition temperatures and associated volume variations were derived from the results plotted in Figs. 4(*a*) and 4(*b*).

	Bulk Pb	Pb nanoparticles, this work	Pb nanoparticles, previous work (Cheyssac *et al.*, 1988)
Melting temperature (K)	600.1 (Nuclear Science Committee, 2007)	580 ± 1	578
Freezing temperature (K)	489 (Cheyssac *et al.*, 1988)†	433 ± 1	451
$\Delta V/V$ at melting	0.036 (Nuclear Science Committee, 2007)	0.034 ± 0.003	–
$\Delta R_g/R_g$ at melting (for spherical NPs)	0.012 (Nuclear Science Committee, 2007)	0.013 ± 0.002	–

† This temperature was obtained extrapolating data from Cheyssac *et al.* (1988).

temperatures. These are the only well defined discontinuities in the integrated SAXS intensity Q and radius of gyration R_g observed under cooling. Taking into account equation (5) and considering that $\rho_{np} > \rho_m$, the observed sharp increase in $Q(T)$ while cooling implies a decrease in nanoparticle volume, $V_{np}(T)$. This transformation from less compact particles (with larger volume) to more compact particles (with smaller volume) was then assigned to the freezing transition of the liquid Pb droplets.

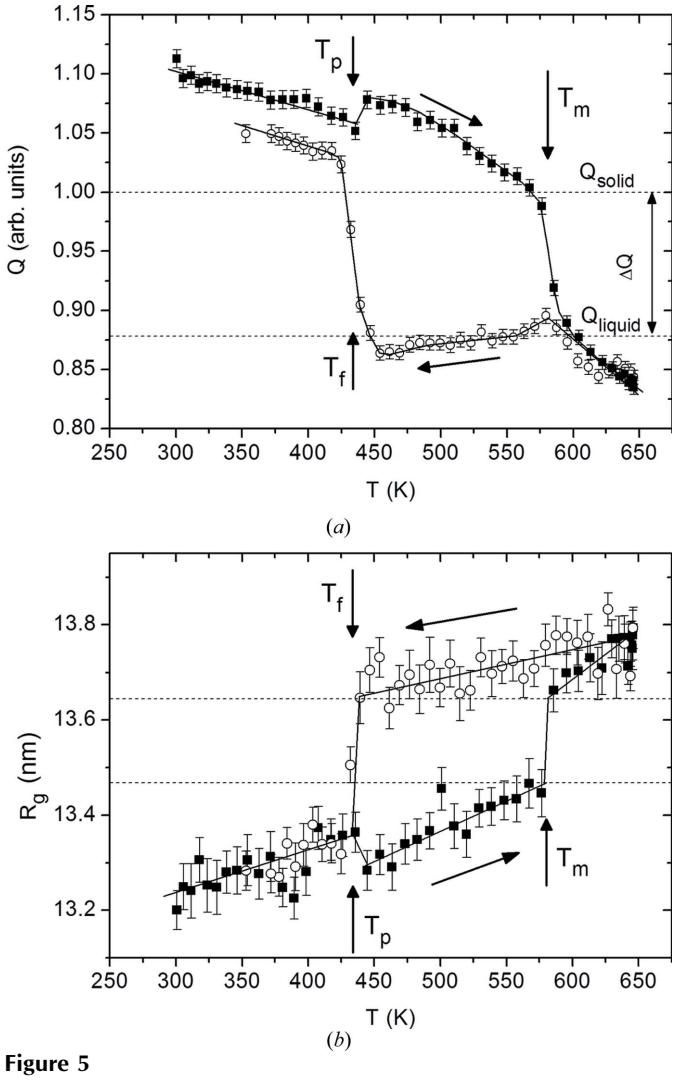

Figure 5
(*a*) Integral of the SAXS intensity in reciprocal space in relative scale, Q, derived by applying equation (3) to the SAXS intensity curves and (*b*) radius of gyration of the Pb nanoparticles, R_g, derived by applying equation (6), as a function of temperature, corresponding to samples submitted to cooling (open symbols) and heating (solid symbols) processes.

On the other hand, during the heating stage of the thermal cycle, a sharp decreasing discontinuity in $Q(T)$ is clearly apparent at T = 580 K (Fig. 5*a*), which, by considering again equation (5), can be associated with a volume increase. Moreover, at the same temperature, $R_g(T)$ also exhibits a sharp increase (Fig. 5*b*). Both observed variations, in $Q(T)$ and $R_g(T)$, are the expected effects produced by the melting of solid Pb nanoparticles.

4.6. Additional structural effects derived from SAXS measurements

We have verified, along the heating stage of the thermal cycle, that the integrated SAXS intensity, $Q(T)$, and the Guinier average of the radii of gyration, $R_g(T)$, of the Pb nanoparticles (Figs. 5*a* and 5*b*, respectively) exhibit an unexpected sharp discontinuity close to T = 433 K, *i.e.* the freezing temperature of the Pb nanodroplets. This jump has also been observed at the same temperature in SAXS intensity $I(q_i,T)$, as can be seen in Fig. 4(*b*). This sharp decrease in the average gyration radius of Pb nanoparticles, under heating, suggests a solid-to-solid transformation involving a transition of the Pb nanoparticles from a less compact to a more close-packed atomic structure.

Another interesting feature of the temperature dependence of the integrated intensity Q, along the cooling stage of the thermal cycle, is its change of slope at the temperature of melting, T_m = 580 K, below which the Pb droplets are in a supercooled liquid state. This change of slope of $Q(T)$ at 580 K is not *a priori* expected for free undercooled nanodroplets.

5. Discussion

Our SAXS results indicate that the melting temperature of Pb nanoparticles with an average radius $\langle R \rangle$ = 16.1 nm is 580 K, *i.e.* a value 20.1 K lower than that of bulk Pb (Table 1). This reduction in the melting temperature is in good agreement with that previously determined for Pb nanoparticles of similar size embedded in an alumina matrix by using an optical method combined with TEM (Cheyssac *et al.*, 1988). On the

other hand, our results indicate a large difference between the melting and freezing temperatures of these nanoparticles, $\Delta T = 147$ K, this difference being somewhat larger than that previously reported for Pb nanodroplets with the same average size, $\Delta T = 130$ K (Cheyssac *et al.*, 1988). This discrepancy is probably due to a difference in the surface energies of the Pb/PbO–B_2O_3–SnO_2 glass and Pb/Al_2O_3 interfaces. The effect of interface energy on melting and freezing temperatures of nanoparticles has been discussed by several authors (Couchman & Jesser, 1977; Allen *et al.*, 1980; Sheng *et al.*, 1998; Saka *et al.*, 1988).

It is worth mentioning that the melting and freezing temperatures of nanoparticles embedded in homogeneous matrices, T_m and T_f, respectively, could be affected by the eventual existence of compressive stresses (Allen *et al.*, 1980). Such stresses may develop, for example, when liquid nanodroplets in a solid matrix formed at high temperature and then cooled to lower temperatures expand at the freezing transition, T_f, as occurs in the case of Bi nanoparticles in glass (Itoigawa *et al.*, 1997). The same effect may also occur during the growth of nanoparticles embedded in a solid matrix at temperatures at which the mobility of the matrix atomic species is much lower than the mobility of solute atoms (Schmelzer *et al.*, 1990; Schmelzer & Möller, 1992). Since the Pb nanoparticles studied here contract on cooling at the freezing transition, T_f, no compressive stresses and strains at this transition are expected to develop. On the other hand, in the nanocomposite investigated here, the temperature of heat treatment at which Pb droplets are formed ($T_{iso} = 716$ K) is higher than the glass transition temperature of the glass matrix, namely $T_g = 665$ K. Therefore, since $T_{iso} > T_g$ a quick relaxation of stresses during the growth of Pb nanodroplets is expected. Furthermore, the linear thermal expansion coefficient of lead–borate glass, $\alpha_g = 9.2 \times 10^{-6}$ K^{-1} (Bobkova, 2003), is lower than that of liquid Pb, $\alpha_{Pb} = 3.7 \times 10^{-5}$ K^{-1} (Nuclear Science Committee, 2007). Therefore, when the composite is cooled from the temperature of formation of Pb droplets (716 K) down to temperatures at which Pb nanoparticles melt and freeze, 580 and 433 K, respectively, the contraction rate of Pb droplets is higher than that of the glass matrix, thus avoiding the development of compressive stresses. We can conclude that compressive stresses on Pb nanoparticles are negligible or absent during the cooling part of the thermal cycle, and therefore this effect is not expected to significantly affect their melting and freezing temperatures.

In the case of bulk Pb the values of the specific masses of the crystalline and liquid phases at the melting temperature are 11.034 and 10.640 g cm^{-3}, respectively (Nuclear Science Committee, 2007). The specific mass of the glass investigated here is equal to 5.87 g cm^{-3} (Singh *et al.*, 2004). The relative variation in volume is related to the relative variation in electron density by $\delta V_{np}/V_{np} = -\delta\rho_{np}/\rho_{np}$. The relative volume variation on heating calculated from this relation using the values mentioned above, at the melting temperature, results in $\delta V_{np}/V_{np} = +0.036$. Moreover, in the simple case of spherical nanoparticles, the relative increase of their radius is expected to be $\delta R/R = (\delta V_{np}/V_{np})/3 = +0.012$.

The horizontal dashed lines plotted in Fig. 5(*a*) indicate the Q values of solid and liquid Pb nanoparticles before and after the solid-to-liquid transition during the sample heating stage. The relative variation in nanoparticle volume $\Delta V/V$ determined from the discontinuity of the integrated SAXS intensity $\Delta Q/Q$ using equation (5) is equal to 0.034 ± 0.003, this value being close to that expected for bulk Pb. The average Guinier radii of Pb nanoparticles before and after the Pb nanoparticles melt are indicated by the dashed lines in Fig. 5(*b*). The relative variation in the average Guinier radius in the solid-to-liquid transition determined from these values is $\Delta R_g/R_g = 0.013 \pm 0.002$.

The values of the melting and freezing temperatures and relative variations of nanoparticle volume at these transitions are summarized in Table 1, together with the same parameters corresponding to bulk Pb.

Another sharp decrease observed in the volume of the Pb nanoparticles during the heating stage of the thermal cycle, at 433 K, associated with the sharp increases in $Q(T)$ (Fig. 5*a*) and $I(q_i,T)$ (Fig. 4*b*) and with the decrease in $R_g(T)$ (Fig. 5*b*), is not *a priori* expected.

The unexpected positive discontinuities in SAXS intensity (Fig. 4*b*) and integral Q (Fig. 5*a*) and abrupt negative variation of the radius of gyration (Fig. 5*b*), on heating, at $T_p = 433$ K, indicate that at this temperature a sharp variation of nanoparticle volume occurs. In order to explain this feature we have considered that, under the preceding cooling process, a fraction of Pb liquid nanodroplets (L phase), instead of transforming into the expected stable crystalline phase (C phase), transform into a metastable disordered frozen phase which is less compact than the crystalline phase (D phase). Moreover the rate of nucleation of the stable Pb nanocrystals inside the disordered phase at temperatures below $T_f = 433$ K can be rather high but, conversely, their rate of growth is expected to be low. During the following heating cycle, the disordered frozen nanoparticles (D phase) melt at their freezing temperature ($T = 433$ K) and, simultaneously, nuclei of the stable crystalline phase formed at lower temperatures grow inside the liquid phase, thus completing the whole $D \rightarrow L \rightarrow C$ transformation within a narrow temperature range. The formation of an intermediary phase instead of the expected stable crystalline phase on cooling has been previously observed in molecular crystals (Craievich *et al.*, 1978) and in CuCl nanocrystals embedded in glass subjected to a heating/cooling thermal cycle (Valov & Leiman, 1997). In these cases the unexpected features observed in thermal analyses under heating, at the freezing temperature, were also assigned to a complex transformation on heating, from a less dense and disordered solid phase to a liquid phase and immediately to the stable crystalline phase. Since SAXS is a low-resolution technique, in order to study the crystallographic details of the metastable disordered phase (D phase), additional studies by using X-ray and/or electron diffraction techniques are required.

A complex transition similar to that described above probably occurs for the Pb nanoparticles embedded in glass studied here. However, in order to confirm the presence and

establish the detailed features of this transition for the studied Pb nanoparticles, additional experimental evidence is required.

Another interesting feature apparent in Fig. 5(*a*) is the change in slope of the integral $Q(T)$, along the cooling stage of the thermal cycle, when the sample is cooled below the melting temperature of Pb nanocrystals. A quantitative determination of the relation between the integral of the SAXS intensity, $Q(T)$, and the nanoparticle volume $V_{np}(T)$ far from the transitions is not straightforward because it depends on the variation with temperature of the electron densities of nanoparticles, $\rho_{np}(T)$, and the glass matrix, $\rho_m(T)$, which are not known. In any case the change of slope of $Q(T)$ observed in Fig. 5(*a*) at the melting temperature, during the cooling stage of the thermal cycle, is not expected for a simple model of free undercooled liquid nanodroplets. This suggests that the change of slope in the integral $Q(T)$ is related to some structural effect promoted by differences in the thermal expansion coefficients of Pb nanoparticles and the glass matrix, which affect the temperature dependence of the size and/or density of the Pb nanodroplets. In order to characterize quantitatively this effect and to determine the structure of the solid phases mentioned above, additional SAXS and TEM investigations are required.

The method used in this work for precise determination of the solid-to-liquid and liquid-to-solid transition temperatures of Pb nanoparticles embedded in a homogeneous glass – based on results from SAXS measurements – can be applied to other similar systems. Since the transition temperatures usually depend strongly on the size of the nanoparticles, the SAXS procedure described here would lead to precise determinations of the size dependence of the transition temperatures of nanoparticles embedded in a homogeneous (liquid or solid) matrix.

6. Conclusion

We have determined the radius distribution of spherical Pb nanoparticles embedded in a $PbO–B_2O_3–SnO_2$ glass matrix by using the SAXS technique. This material was established to be composed of a homogeneous glass containing Pb nanoparticles with an average radius $\langle R\rangle$ = 16.1 nm and relative radius dispersion $\sigma/\langle R\rangle$ = 0.10.

We have also determined the melting and freezing temperatures of Pb nanoparticles from the measurements of the temperature dependence of the integral of SAXS intensity in reciprocal space, $Q(T)$, and the radius of gyration, $R_g(T)$, derived by applying the Guinier law. The freezing and melting temperatures of these nanoparticles were determined to be 433 and 580 K, respectively.

An additional, unexpected contraction of the nanoparticles on heating, at 433 K, indicates that the frozen Pb nanoparticles suffer a transition to a more compact phase before melting at a higher temperature (580 K). To achieve a more detailed characterization of the structural features of the observed structural transition at 433 K, additional experimental evidence from TEM and/or thermal analyses are required.

The results of this work demonstrate that the melting and freezing temperatures of nanoparticles in a very diluted state, for which the X-ray diffraction technique is not sensitive enough, can be precisely determined by applying only the SAXS method.

This work was supported by CNPq (the Brazilian funding agency), Universal 478100/2012-4, and by the Brazilian National Synchrotron Light Laboratory (LNLS).

References

Allen, G. L., Gile, W. W. & Jesser, W. A. (1980). *Acta Metall*. **28**, 1695–1701.
Bobkova, N. M. (2003). *Glass Phys. Chem.* **29**, 501–507.
Cheyssac, P., Kofman, R. & Garrigos, R. (1988). *Phys. Scr.* **38**, 164–168.
Couchman, P. R. & Jesser, W. A. (1977). *Nature*, **269**, 481–483.
Craievich, A. F. (2005). *Handbook of Sol–Gel Science and Technology*, Vol. II, ch. 8, edited by A. Sakka, pp. 161–189. Dordrecht: Kluwer Academic Publishers.
Craievich, A. F., Kellermann, G., Barbosa, L. C. & Alves, O. L. (2002). *Phys. Rev. Lett*. **89**, 235503.
Craievich, A. F., Levelut, A. M., Lambert, M. & Albon, N. (1978). *J. Phys.* T**39**, 377–388.
Gonella, F. & Mazzoldi, P. (2000). *Handbook of Nanostructured Materials and Nanotechnology*. New York: Academic Press.
Hamanaka, Y. & Nakamura, A. (1999). *Appl. Phys. Lett*. **75**, 1712–1714.
Itoigawa, H., Kamiyama, T. & Nakamura, Y. (1997). *J. Non-Cryst. Solids*, **210**, 95–100.
Kellermann, G. & Craievich, A. F. (2002). *Phys. Rev. B*, **65**, 134204.
Kellermann, G. & Craievich, A. F. (2008). *Phys. Rev. B*, **78**, 054106.
Kellermann, G., Craievich, A. F., Neuenschwander, R. & Plivelic, T. S. (2003). *Nucl. Instrum. Methods Phys. Res. Sect. B*, **199**, 112–116.
Kofman, R., Cheyssac, P. & Garrigos, R. (1990). *Phase Transitions*, Vols. 24–26, pp. 283–342. London: Gordon and Breach.
Lopeandia, A. F. & Rodrıguez-Viejo, J. (2007). *Thermochim. Acta*, **461**, 82–87.
Mazzoldi, P., Arnold, G. W., Battaglin, G., Gonella, F. & Haglund, R. F. (1996). *J. Nonlinear Opt. Phys. Mater*. **5**, 285–330.
Nogami, M. & Abe, Y. (1994). *Appl. Phys. Lett*. **65**, 2545–2547.
Nuclear Science Committee (2007). *Handbook on Lead–bismuth Eutectic Alloy and Lead Properties, Materials Compatibility, Thermal-hydraulics and Technologies*, edited by the OECD Nuclear Energy Agency.
Pavesi, L., Dal Negro, L., Mazzoleni, C., Franzo, G. & Priolo, F. (2000). *Nature*, **408**, 440–444.
Saka, H., Nishikawa, Y. & Imura, T. (1988). *Philos. Mag. A*, **56**, 895–906.
Schmelzer, J. & Möller, J. (1992). *Phase Transitions*, **38**, 261–272.
Schmelzer, J., Pascova, R. & Gutzow, I. (1990). *Phys. Status Solidi (a)*, **117**, 363–375.
Sheng, H. W., Lu, K. & Ma, E. (1998). *Acta Mater*. **46**, 5195–5205.
Singh, N., Singh, K. J., Singh, K. & Singh, H. (2004). *Nucl. Instrum. Methods Phys. Res. Sect. B*, **225**, 305–309.
Strunz, P. M., Mukjerji, D., Gilles, R., Geue, T. & Rosler, J. (2012). *J. Phys. Conf. Ser.* **340**, 012098.
Takagi, M. (1954). *J. Phys. Soc. Jpn*, **9**, 359–363.
Valov, P. M. & Leiman, V. I. (1997). *JETP Lett.* **66**, 510–516.
Yang, H., Huang, D., Wang, X., Gu, X., Wang, F., Xie, S. & Yao, X. (2005). *J. Nanosci. Nanotechnol*. **5**, 1737–1740.
Zhao, M., Zhou, X. H. & Jiang, Q. (2001). *J. Mater. Res.* **16**, 3304–3308.